

Scalable semi-classical implementation of Shor factoring using time-multiplexed degenerate optical parametric oscillators

Minghui Li, Wei Wang, Zikang Tang, and Hou Ian

*Institute of Applied Physics and Materials Engineering,
University of Macau, Macau S.A.R., China*

A scheme to encode arbitrarily long integer pairs on degenerate optical parametric oscillations multiplexed in time is proposed. The classical entanglement between the polarization directions and the phases of the oscillating pulses, regarded as two computational registers, furnishes the integer correlations within each pair. We show the major algorithmic steps, modular exponentiation and discrete Fourier transform, of Shor's quantum factoring algorithm can be executed in the registers as pulse interferences under the assistance of external logics. The factoring algorithm is thus rendered equivalent to a semi-classical optical-path implementation that is scalable and decoherence-free. The sought-after multiplicative order, from which the prime factors are deduced, is identified from a two-dimensional fringe image generated by four-hole interference measured at the end of the path.

I. INTRODUCTION

Since the now renowned quantum integer factoring algorithm was proposed by Shor more than two decades ago [1], experimental implementations of its compiled versions have been demonstrated on various platforms, include those on nuclear magnetic resonance (NMR) systems [2], photonic systems [3, 4], superconducting circuits [5], and ion-trap systems [6]. Despite these demonstrations, a scalable quantum computer that runs Shor's algorithm still remains a distant goal that challenges many researchers in the field.

For instance, the scalability challenge for an NMR system is posed by the fact that the qubits are encoded in the mixed states of magnetic spins within one molecule, making the system detectable only through an exponentially scaling number of measurements on the entire ensemble of the spins [7]. Using photons as qubits, recycling techniques has helped to reduce the n qubits needed by the control register to a single qubit [8], but the number of qubits in the work register remains the same. Furthermore, due to low brightness and low collection efficiency, scaling photon entanglement is still challenging, although great efforts have led to an ever greater demonstrated number of entangled photons in recent years [9, 10]. In contrast, forming qubits in ion-trap systems or superconducting circuits is lesser of a problem [6, 11]. Nevertheless, other experimental difficulties

arise. For ions trapped inside optical or magnetic wells, qubit control is realized through focused laser pulses, making the coupling efficiency depend on the efficacy of fine focusing. The recent invent of on-chip ion traps has partially remedied this problem [12, 13]. For superconducting circuits, limited coherence times of the superconducting qubits, though current technologies has pushed them well beyond the order of μs [14], mandates the use of quantum error correction for scaling [15]. The error-correcting protocols in turn demand the employment of auxiliary qubits, which spatially complexify the circuit design [16, 17].

Moreover, despite the experimental verifications of Shor's algorithm across diversified physical systems discussed above [2–6], the key algorithmic step of computing modular exponentiation often still has to rely on external resources when the multiplicative order is long [18]. The title of a full-fledged integer-factoring quantum computer is yet to be claimed. While anticipating the solutions to the obstacles discussed, we propose here a semi-classical implementation of Shor's algorithm where the probabilistic nature of full quantum systems is removed but the characteristics of entangled states retained, using classical entanglement.

In optics, quantum entangled states are established between a pair of photons when detections are made by on photodiodes; whereas, classical entangled states exist among two degrees of freedom within a single macroscopic light beam [19, 20], detectable by interference fringe patterns [21]. The inseparable correlations are established classically between the polarization direction and either the amplitude [20], or the spatial parity [22], or the position [23] of a light beam. Given the inseparation, violations of Bell-like inequalities have been demonstrated [24, 25]. On the theoretical side, Schmidt analysis intended for quantifying pure-state entanglement [26] is generalized to classical fields [20, 21]. These studies suggest that, stripping away the non-locality inferred by the Einstein-Podolsky-Rosen experiment, classical entanglement plays an substituting role in indicating local non-classical correlation. Free from decoherence, the long-life classical analogue is also proved to be detrimental to implementing the Deutsch algorithm [27], quantum walk [28], and the quantum Fourier transform [29] without a quantum system.

Our proposal encodes the classically entangled bits between the phase states, $|0\rangle$ and $|\pi\rangle$, and the polarization direction states, $|H\rangle$ (horizontal) and $|V\rangle$ (vertical), in degenerate optical parametric oscillators (DOPOs) [30]. These oscillators being essentially phase-coherent single-mode pulses are free from state decoherence while propagating in fibers, although their intensities need to be compensated through regular amplification. Their phase coherence and ability to be time multiplexed [31, 32] earn them a key role in carrying out quantum annealing algorithms in coherent Ising machine [33, 34]. Here, we use the time multiplexity to scale the number of bits necessary

to store the computing data of Shor's algorithm, where the two entangled degrees of freedom are allocated to, respectively, the control and the work registers. Though the semi-classical approach does not have concurrence implied by quantum superposition states, it is scalable and simplifies the algorithm by eliminating the step of quantum Fourier transform (QFT), which is implemented by concatenated phase gates. Instead, the QFT is effectively merged with the last measurement step through interference pattern detection [21], which not only substitutes the projective measurements for quantum implementation, but also absorbs the transform process.

In the following, we explain the theoretical model in Sec. II, demonstrate the simulation results of the interference patterns that carry computational significance in Sec. III. The details of proposed experimental setup are given in Sec. III and the conclusions are given in Sec. IV.

II. THEORETICAL MODEL

The computational bits are encoded in time-multiplexed degenerate optical parametric oscillators (DOPOs), which are essentially traveling narrow-width pulses in a free space or fiber cavity. When pumped well above a power threshold and maintained by a nonlinear crystal such as a periodically poled lithium niobate (PPLN), each DOPO pulse sustains a 0 or π phase relative to the pump pulse due to phase sensitive amplification [35]. These phase states constitute the first pair of encoding bits $|0\rangle$ and $|1\rangle$, to be used for the control register in the algorithm. Simultaneously, each DOPO carries a fixed polarization direction, which can be maintained freely in space or through a polarization-preserving fiber for a fiber cavity. Thus, the independent horizontal and vertical polarizations constitute the second pair of encoding bits for the work register. Throughout their propagation in an optical cavity, particular correlations among the phase bits and the polarization bits are subsisted without extra manipulations, allowing entangled computational data to be stored in the DOPOs.

As shown in Fig. 1, the computational steps of Shor's algorithm are accomplished by inserting DOPO manipulating elements in the optical cavity, with which the information storing pulses are read out or interfered with correction pulses for data write-in. Particularly, the modular exponential function (MEF) step relies on an external field-programmable grid array (the FPGA2 module) to compute the exponentiation in electrical pulse signals, which are then fed into the control ports of a pair of optical switches as inverted signals to produce correlations between phases and polarization directions of the incident pulses. The QFT has been performed on classical optical fields using phase modulation of beams (Cf. Ref [29]), which demands costly resources when scaling up. In the

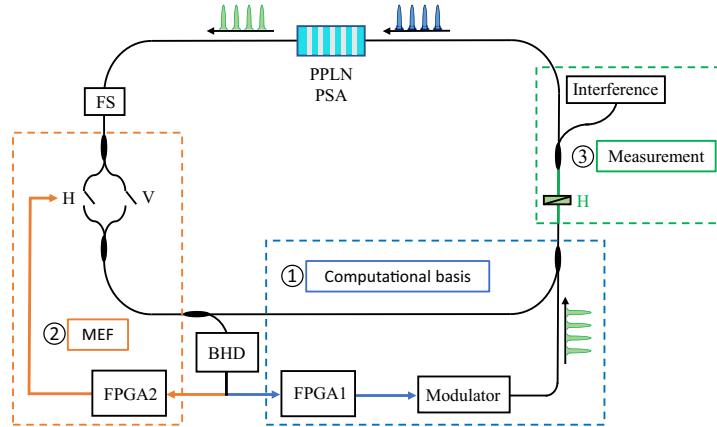


FIG. 1. Setup design of a classical implementation of Shor’s algorithm. PPLN, periodically poled lithium niobate; FS, fiber stretcher; PSA, phase sensitive amplification; BHD, balanced homodyne detector; FPGA, field programmable gate array; Modulator, a module contains the phase modulator and the intensity modulator.

proposed setup with DOPOs here, direct interference measurement on the phases are permitted without quantum projective collapse, whose fringe patterns implies the transformation results. Therefore, no particular optical elements are needed to execute QFT in the optical cavity, as illustrated in the figure. Before we discuss the details of the experimental design in Sec. IV, we study how Shor’s algorithm can be embedded into the DOPO-filled cavity below.

To realize the quantum factoring of a composite number $N = pq$, with p and q are odd primes, one randomly chooses a base a ($0 < a < N$) which is coprime to N . Then, one computes the multiplicative order r of the MEF $f(x) = a^x \text{mod} N$, which is the minimum integer that satisfies $a^r \text{mod} N = 1$. For an even r , at least one prime factor is given by the greatest common divisor (GCD) of $a^{r/2} \pm 1$ and N .

The quantum circuits of Shor’s algorithm involve at least two registers: the control register with $n = 2 \lceil \log_2 N \rceil$ qubits to store the numbers x and the work register with $m = \lceil \log_2 N \rceil$ qubits to store the values of $f(x)$. The control register is initialized as $|0\rangle$ and the work register is initialized as $|1\rangle$ in computational basis representation. Applying the Hadamard transform on the control register, it becomes $2^{-n/2} \sum_{x=0}^{2^n-1} |x\rangle$, which is a superposition state of all computational basis states. Controlled unitary operations for implementing the MEF on the work register entangle each input value x and the corresponding value $f(x)$. The entanglement is necessary for speedup in quantum factoring. Subsequently, the QFT is applied on the control register, which results in peaks at values of $k2^n/r$ (for integer k). Finally, the multiplicative order r can be found by

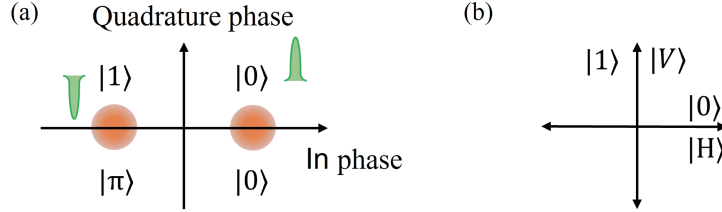


FIG. 2. Information encoded by the state of a DOPO. (a) Representation of a classical bit in the control register with the phase state of a DOPO. (b) Representation of a classical bit in the work register with the polarization state of a DOPO.

observing the control register.

For the general case, we assume that the integer to be factored is N and the base is a . The control register and work register require $n = 2 \lceil \log_2 N \rceil$ and $m = \lceil \log_2 N \rceil$ qubits, respectively. It means we need to prepare computational basis states from $|0\rangle$ to $|2^n - 1\rangle$. In order to encode information in the form of binary numbers, we need physical quantity with binary values. It has been demonstrated that the state of a DOPO is a coherent state when pumped above the threshold. The phase of the coherent state is either 0 or π due to phase sensitive amplification. For a single DOPO, we use its phase states, 0 or π , to represent the states of a classical bit, $|0\rangle$ or $|1\rangle$, in the control register (Fig. 2(a)). Thus, n time-multiplexed DOPOs as a group are required to represent a n -bit number, for example, we can use the phase states of a group of DOPOs $|0\pi0\pi \cdots 0\pi\rangle_n$ to represent the binary number $|0101 \cdots 01\rangle_n$. At the same time, we use the H or V polarization of a DOPO to represent the states of a classical bit, $|0\rangle$ or $|1\rangle$, in the work register (Fig. 2(b)), for example, we can use the polarization states of a group of DOPOs $|HVHV \cdots HV\rangle_n$ to represent the binary number $|0101 \cdots 01\rangle_n$. Since the number of DOPOs is extensible, the experimental scalability of simulating Shor's algorithm has been realized.

For a DOPO operating above the threshold, its phase state is either 0 or π . We skip the Hadamard transform and prepare an input initial state straightly. The initial state of the DOPO network is prepared as:

$$|\psi_0\rangle = \frac{1}{\sqrt{2^n}} \sum_{j=0}^{2^n-1} |j, 0\rangle, \quad (1)$$

which is a product of the superposition of all computational basis states in the control register and $|0\rangle$ in the work register.

The implementation of MEF in quantum circuit can be decomposed to controlled multiplications [36]. While feasible in principle, the number of qubits and quantum gates required is difficult to achieve. The computation process has been completed in a “black-box” fashion in compiled versions of Shor’s algorithm [6]. Here, we adopt the Montgomery multiplication algorithm [37] on a field-programmable gate array (FPGA) to compute the MEF. The Montgomery multiplication uses a representation of residue classes for speedup. For an integer N , select an integer R which satisfies $R > N$ and $\text{GCD}(R, N) = 1$. Through extended Euclidean algorithm, we can obtain two integers R^{-1} and N' satisfying $0 < R^{-1} < N$ and $0 < N' < R$ and $RR^{-1} - NN' = 1$. With these auxiliary numbers, the Montgomery multiplication computes:

$$\text{Mont}(t_1, t_2) = t_1 \cdot t_2 \cdot R^{-1} \pmod{N}, \quad (2)$$

where t_1, t_2 are integers satisfying $t_1, t_2 < N$. When R is taken to be a power of 2, the Montgomery multiplication algorithm can avoid trial divisions, which makes it faster than ordinary modular multiplication [38]. Specifically, the MEF is decomposed to repeated squaring and modular multiplication by binary method [36]:

$$a^x \pmod{N} = \prod_{j=1}^n a^{x_{n-j} 2^{n-j}} \pmod{N}. \quad (3)$$

The base a is converted to an N -residue for computation, which is defined as $\bar{a} = aR \pmod{N}$. When computing modular multiplication with Eq. (2), the modular operation can be replaced by bit shift and bit-wise AND operations, which are fast in classical computers. All repeated squaring and modular multiplications are conducted in the N -residue system. By converting the iterative result of Eq. (3) out of the N -residue system, the value of MEF is acquired. The FPGA computes the squaring and multiplication according to the input value x , which is represented by the phase states of a group of n sequential DOPOs. The values of MEF are stored in the polarization states of the same group of DOPOs. For the convenience of the following measurement experiment, we change the MEF value to $a^x \pmod{N} - 1$. The state of the DOPO network becomes a classical entangled state:

$$|\psi_1\rangle = \frac{1}{\sqrt{2^n}} \sum_{j=0}^{2^n-1} |j, a^j \pmod{N-1}\rangle. \quad (4)$$

The degree of entanglement of $|\psi_1\rangle$ can be quantified by the Schmidt number K .

In order to find the multiplicative order contained in the control register, we need to measure the work register first. In general, n polarizers are required to select a random MEF value represented by the polarization states of a DOPO group. But for simple demonstration, we use only one horizontal polarizer to measure the work register first. As a result, all DOPOs with vertical polarization are eliminated. Since we treat n sequential DOPOs as a group, only those values of MEF represented by $|HH \cdots H\rangle_n$ polarization state are kept unchanged. So the state of the DOPO network becomes:

$$|\psi_2\rangle = \frac{1}{\sqrt{2^M}} \sum_{j=1}^M |x_j, 0\rangle, \quad (5)$$

where M is the number of input values whose MEF is equal to 1. Apparently, the state $|\psi_2\rangle$ is a product state. If we can read all the values in the control register, the multiplicative order can be found. However, for quantum computer, measurement will lead to collapse of the superposition state in the control register, which hinders further measurement. Hence, the QFT is applied on the control register to read out the multiplicative order [36].

Consider for a specific case with $N = 15$ and $a = 7$ for executing the algorithm. We have $n = 8$ and $m = 4$. However, $n = 4$ qubits are enough for the control register due to the multiplicative order r in this situation is 4 [3]. Consequently, a network of 64 DOPOs is required to represent all the computational basis. We can rewrite $|\psi_1\rangle$, with orthonormal basis in phase and polarization degrees of freedom, in a classical perfectly organized form [20]:

$$\begin{aligned} |\psi_1\rangle = & \frac{1}{2} \left[\frac{1}{2} (|00\rangle + |0\pi\rangle + |\pi 0\rangle + |\pi\pi\rangle) |00\rangle \right] \otimes |HHHH\rangle \\ & + \frac{1}{2} \left[\frac{1}{2} (|00\rangle + |0\pi\rangle + |\pi 0\rangle + |\pi\pi\rangle) |0\pi\rangle \right] \otimes |HVVH\rangle \\ & + \frac{1}{2} \left[\frac{1}{2} (|00\rangle + |0\pi\rangle + |\pi 0\rangle + |\pi\pi\rangle) |\pi 0\rangle \right] \otimes |HHVV\rangle \\ & + \frac{1}{2} \left[\frac{1}{2} (|00\rangle + |0\pi\rangle + |\pi 0\rangle + |\pi\pi\rangle) |\pi\pi\rangle \right] \otimes |VVHH\rangle. \end{aligned} \quad (6)$$

So the Schmidt number is $K = 1/(4 \times 2^{-4}) = 4$, which is equal to the multiplicative order of MEF. In particular, the degree of entanglement will increase with the multiplicative order. It shows that an extensible degree of entanglement is also necessary for scalable Shor's algorithm. After measurement of the work register, the state of the DOPO network becomes:

$$|\psi_2\rangle = \frac{1}{2} (|0\rangle + |4\rangle + |8\rangle + |12\rangle) |0\rangle. \quad (7)$$

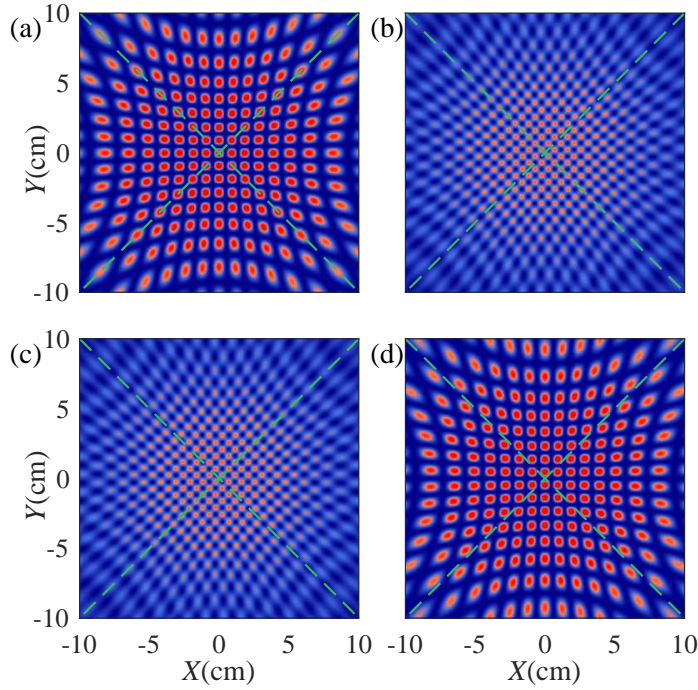


FIG. 3. Simulation results of measurement through four-hole interference patterns. The phase states of a group of DOPOs are: (a) $|0000\rangle$, (b) $|0\pi00\rangle$, (c) $|\pi000\rangle$, (d) $|\pi\pi00\rangle$.

Since the measurement will not result in a collapse of the register state for classical implementation, we can directly measure the control register. We separate a group of DOPOs into four holes for interference [21] through delay lines, so the phase states of 4 DOPOs can be read at the same time. Even though some groups only contain two DOPOs, they can also form interference patterns with stripes. Nevertheless, those intact groups can form interference patterns with bright or dark spots. All the interference patterns of these temporally separated DOPO groups form a video that contains 16 frames, as shown in the Supplementary Video. The interference patterns are distinguished through their symmetry character(Fig. 3). From the phase states of a group of DOPOs, we derive four values: 0, 4, 8, and 12. The multiplicative order is deduced to be $r = 4$. Therefore, the prime factors of N could be obtained.

III. EXPERIMENTAL REALIZATION

The experiment setup to simulate a scalable version of Shor's algorithm is based on a network of time multiplexed DOPOs [34] combined with computation and measurement parts. Fig. 1 shows the schematic, which mainly contains three parts. The laser is a continuous wave laser with a

wavelength of 1536 nm, which is suitable for dispersion-shifted fiber. The laser output is split into two paths, one of which is phase-modulated and used as a local oscillator for the BHD, and another one is modulated by an intensity modulator for pulse generation. The generated pulse train with a repetition multiplicative order of T_{rep} is further split into two paths. One path is launched to the modulator module to generate the feedback pulses according to the feedback signal from FPGA1. The other is used to synchronously pump the PPLN for phase sensitive amplification after the second harmonic generation process is completed by another PPLN.

One DOPO is formed with the PPLN and a fiber-ring cavity. For realizing a network of time multiplexed DOPOs, we set the round trip time as $T_{\text{rt}} = 60T_{\text{rep}}$. The PSA process is designed with type 0 phase matching ($e \rightarrow e + e$), so that the DOPOs are generated with horizontal polarization. In the beginning, the optical switch allowing for horizontal polarization is connected, so that the DOPOs can operate continuously. To maintain the phase state of each DOPO, the FS is used to stabilize the length of the cavity. As a result, the phase difference between two pump pulses of the same signal pulse is compensated by the cavity length, so that the signal pulse and the pump pulse are synchronous and the relative phase difference between them is fixed at 0 or π .

To prepare the computational basis, we use the BHD to measure the in-phase component c_j of DOPOs and the measurement results are sent to FPGA1. The phase state of a DOPO is treated as 0 or π when c_j is positive or negative, respectively. The phase state of a DOPO is randomly 0 or π , so we need to change it to the set value required for preparing the computational basis. FPGA1 computes the feedback signal $f_j = -2(1 - \delta_{ij})c_j$, where δ_{ij} means comparing the phase state of j th DOPO and i th set value shown in Fig. 4(a). The 0 or π phase state means the quadrature component of a DOPO is zero and therefore the coupling pulse only controls the in-phase component of it. When $f_i = -2c_j$, the phase of the coupling pulse is π relative to the DOPO, which is realized by phase modulation. Then, the feedback signal synchronously controls the coupling pulses through an intensity modulator, so that all the phase states of DOPOs become the same as the set values.

The implementation of MEF relies on FPGA2 and two optical switches. After the superposition state of all computational basis is prepared, FPGA2 receives the phase states of a group of DOPOs and computes the MEF through Montgomery multiplication in one round. The values of MEF are stored in the polarization states of the same group of DOPOs in the next round. The stored procedure is completed by two optical switches which allow for horizontal and vertical polarization, respectively. The state of the DOPO network after MEF is shown in Fig. 4(b).

The measurement part contains two steps: first, a polarizer is used to select all horizontal

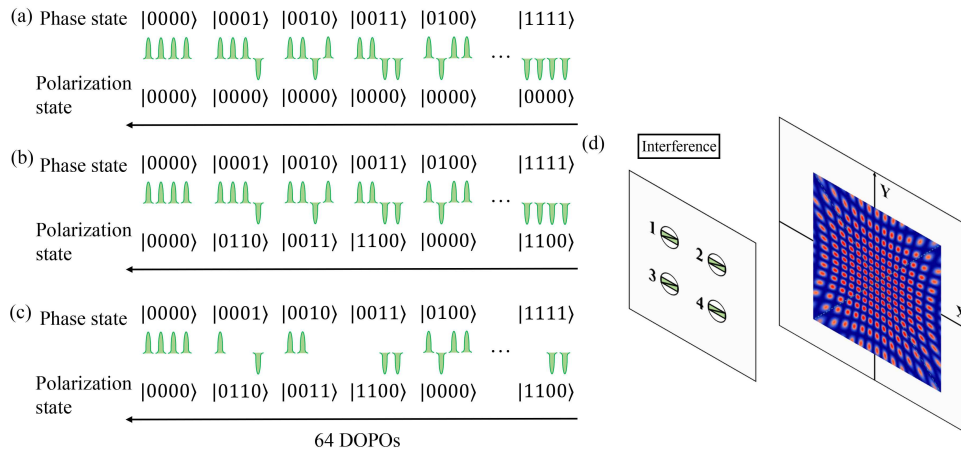


FIG. 4. The states of DOPOs. (a) Initial state of the DOPO network. (b) State of the DOPO network after MEF. (c) State of the DOPO network after measurement of a horizontal polarizer. (d) A general design for measurement.

polarized DOPOs (Fig. 4(c)); second, a four-hole interference is exploited to measure the values represented by a group of DOPOs. The DOPOs are split, through a coupler, into four paths, which have different delay times so that a group of DOPOs can arrive at the screen simultaneously. Finally, we can read the results through interference patterns. A general four-hole measurement design is shown in Fig. 4(d). Four adjustable polarizers are fixed at four holes, respectively. The selection of different MEF values could be completed through change of the polarizers to be horizontal or vertical. Subsequently, the phase states of a DOPO group are derived through the interference patterns.

IV. CONCLUSIONS

We have proposed a scalable implementation of Shor's algorithm using an entirely classical optical system. Specifically, the degrees of freedoms from the phase and the polarization direction of DOPOs were used to represent the entangled bits of the algorithmic control and work registers, making the design free from decoherence innate to qubit systems. Stored as an order pulse train in a ring cavity, e.g. an optical fiber, the DOPOs are interfered with oscillating pulses produced by external optical switches and FPGA logics to execute the key steps of modular exponentiation and discrete Fourier transform. The oscillating pulses of fixed width are multiplexed in time while

running along the cavity length. Any bit length needed by the input integer can therefore be accommodated by sufficient cavity length and pulse amplification, making the implementation scalable.

This implementation is semi-classical because the entangled degrees of freedom permit half-parallel operations on the integers stored. Manipulations on the phases are immediately reflected in the accompanying polarization directions although the bits represented by the full pulse train are operated on one by one in time. We note that the time multiplexing that scales linearly with the bit length are only hardware bounded, i.e. the retention conditions of a fiber as the ring cavity. From the perspective of computation, its scaling is accounted by space complexity only and not related to query or time complexity. Although the classical parametric oscillators are unable to form superposition states and perform projective measurements for full parallelism characteristic of quantum systems, the major concern over time complexity by Shor and other factoring algorithms is indeed addressed. Finally, the computed registers are read by sending the polarized beams of the DOPOs through a four-hole interference. The fringe patterns are uniquely mapped to the multiplicative order sought by the algorithm, where the generation and mapping does not contribute to the algorithmic complexity.

-
- [1] P. Shor, “Polynomial-Time Algorithms for Prime Factorization and Discrete Logarithms on a Quantum Computer,” *SIAM J. Comput.* **26**, 1484 (1997).
 - [2] L. M. K. Vandersypen, M. Steffen, G. Breyta, C. S. Yannoni, M. H. Sherwood, and I. L. Chuang, “Experimental realization of Shor’s quantum factoring algorithm using nuclear magnetic resonance,” *Nature* **414**, 883 (2001).
 - [3] C.-Y. Lu, D. E. Browne, T. Yang, and J.-W. Pan, “Demonstration of a Compiled Version of Shor’s Quantum Factoring Algorithm Using Photonic Qubits,” *Phys. Rev. Lett.* **99**, 250504 (2007).
 - [4] B. P. Lanyon, T. J. Weinhold, N. K. Langford, M. Barbieri, D. F. V. James, A. Gilchrist, and A. G. White, “Experimental Demonstration of a Compiled Version of Shor’s Algorithm with Quantum Entanglement,” *Phys. Rev. Lett.* **99**, 250505 (2007).
 - [5] E. Lucero, R. Barends, Y. Chen, J. Kelly, M. Mariantoni, A. Megrant, P. O’Malley, D. Sank, A. Vainsencher, J. Wenner, T. White, Y. Yin, A. N. Cleland, and J. M. Martinis, “Computing prime factors with a Josephson phase qubit quantum processor,” *Nat. Phys.* **8**, 719 (2012).
 - [6] T. Monz, D. Nigg, E. Martinez, M. Brandl, P. Schindler, R. Rines, S. Wang, I.-L. Chuang, and R. Blatt, “Realization of a scalable Shor algorithm,” *Science* **351**, 1068 (2016).
 - [7] F. Schmidt-Kaler, H. Häffner, M. Riebe, S. Gulde, G. P. T. Lancaster, T. Deuschle, C. Becher, C.

- F. Roos, J. Eschner, and R. Blatt, “Realization of the Cirac-Zoller controlled-NOT quantum gate,” *Nature* **422**, 408 (2003).
- [8] E. Martín-López, A. Laing, T. Lawson, R. Alvarez, X.-Q. Zhou, and J. L. O’Brien, “Experimental realization of Shor’s quantum factoring algorithm using qubit recycling,” *Nat. Photonics* **6**, 773 (2012).
- [9] X.-L. Wang, L.-K. Chen, W. Li, H. L. Huang, C. Liu, C. Chen, Y. H. Luo, Z. E. Su, D. Wu, Z. D. Li, H. Lu, Y. Hu, X. Jiang, C. Z. Peng, L. Li, N. L. Liu, Y.-A. Chen, C.-Y. Lu, and J.-W. Pan, “Experimental Ten-Photon Entanglement,” *Phys. Rev. Lett.* **117**, 210502 (2016).
- [10] X.-L. Wang, Y.-H. Luo, H.-L. Huang, M.-C. Chen, Z.-E. Su, C. Liu, C. Chen, W. Li, Y.-Q. Fang, X. Jiang, J. Zhang, L. Li, N.-L. Liu, C.-Y. Lu, and J.-W. Pan, “18-Qubit Entanglement with Six Photons’ Three Degrees of Freedom,” *Phys. Rev. Lett.* **120**, 260502 (2018).
- [11] R. Barends, J. Kelly, A. Megrant, D. Sank, E. Jeffrey, Y. Chen, Y. Yin, B. Chiaro, J. Mutus, C. Neill, P. O’Malley, P. Roushan, J. Wenner, T. C. White, A. N. Cleland, and J. M. Martinis, “Coherent Josephson Qubit Suitable for Scalable Quantum Integrated Circuits,” *Phys. Rev. Lett.* **111**, 080502 (2013).
- [12] [1]Z. D. Romaszko, S. Hong, M. Siegele, R. K. Puddy, F. R. Lebrun-Gallagher, S. Weidt, and W. K. Hensinger, “Engineering of microfabricated ion traps and integration of advanced on-chip features,” *Nat. Rev. Phys.* **2**, 285 (2020).
- [13] S. L. Todaro, V. B. Verma, K. C. McCormick, D. T. C. Allcock, R. P. Mirin, D. J. Wineland, S. W. Nam, A. C. Wilson, D. Leibfried, and D. H. Slichter, “State Readout of a Trapped Ion Qubit Using a Trap-Integrated Superconducting Photon Detector,” *Phys. Rev. Lett.* **126**, 010501 (2021).
- [14] C. Rigetti, J. M. Gambetta, S. Poletto, B. L. T. Plourde, J. M. Chow, A. D. Córcoles, J. A. Smolin, S. T. Merkel, J. R. Rozen, G. A. Keefe, M. B. Rothwell, M. B. Ketchen, and M. Steffen, “Superconducting qubit in a waveguide cavity with a coherence time approaching 0.1 ms,” *Phys. Rev. B* **86**, 100506 (2012).
- [15] J. Koch, T. M. Yu, J. Gambetta, A. A. Houck, D. I. Schuster, J. Majer, A. Blais, M. H. Devoret, S. M. Girvin, and R. J. Schoelkopf, “Charge-insensitive qubit design derived from the Cooper pair box,” *Phys. Rev. A* **76**, 042319 (2007).
- [16] M. Kjaergaard, M. E. Schwartz, J. Braumüller, P. Krantz, J. I. J. Wang, S. Gustavsson, and W. D. Oliver, “Superconducting Qubits: Current State of Play,” *Annu. Rev. Condens. Matter Phys.* **11**, 369 (2020).
- [17] K. Bharti, A. Cervera-Lierta, T. H. Kyaw, T. Haug, S. Alperin-Lea, A. Anand, M. Degroote, H. Heimonen, J. S. Kottmann, T. Menke, W. K. Mok, S. Sim, L. C. Kwek, and A. Aspuru-Guzik, “Noisy intermediate-scale quantum algorithms,” *Rev. Mod. Phys.* **94**, 015004 (2022).
- [18] J. A. Smolin, G. Smith, and A. Vargo, “Oversimplifying quantum factoring,” *Nature* **499**, 163 (2013).
- [19] R. J. C. Spreeuw, “A Classical Analogy of Entanglement,” *Found. Phys.* **28**, 361 (1998).
- [20] X.-F. Qian and J. H. Eberly, “Entanglement and classical polarization states,” *Opt. Lett.* **36**, 4110 (2011).
- [21] Z. You, Y. Wang, Z. Tang, and H. Ian, “Measurement of classical entanglement using interference

- fringes,” *J. Opt. Soc. Am. B* **38**, 1798 (2021).
- [22] K. H. Kagalwala, G. Di Giuseppe, A. F. Abouraddy, and B. E. A. Saleh, “Bell’s measure in classical optical coherence,” *Nat. Photonics* **7**, 72 (2013).
- [23] A. Aiello, F. Töppel, C. Marquardt, E. Giacobino, and G. Leuchs, “Quantum-like nonseparable structures in optical beams,” *New J. Phys.* **17**, 043024 (2015).
- [24] X.-F. Qian, B. Little, J. C. Howell, and J. H. Eberly, “Shifting the Quantum-Classical Boundary: Theory and Experiment for Statistically Classical Optical Fields,” *Optica* **2**, 611 (2015).
- [25] J. Gonzales, P. Sánchez, D. Barberena, Y. Yugra, R. Caballero, and F. D. Zela, “Experimental Bell violations with classical, non-entangled optical fields,” *J. Phys. B: At. Mol. Op.* **51**, 045401 (2018).
- [26] J. H. Eberly, “Schmidt analysis of pure-state entanglement,” *Laser Phys.* **16**, 921 (2006).
- [27] B. Perez-Garcia, J. Francis, M. McLaren, R. I. Hernandez-Aranda, A. Forbes, and T. Konrad, “Quantum computation with classical light: The Deutsch algorithm,” *Phys. Lett. A* **379**, 1675 (2015).
- [28] S. K. Goyal, F. S. Roux, A. Forbes, and T. Konrad, “Implementing quantum walks using orbital angular momentum of classical light,” *Phys. Rev. Lett.* **110**, 263602 (2013).
- [29] X. Song, Y. Sun, P. Li, H. Qin, and X. Zhang, “Bell’s measure and implementing quantum Fourier transform with orbital angular momentum of classical light,” *Sci. Rep.* **5**, 14113 (2015).
- [30] R. Loudon, *The Quantum Theory of Light* (Clarendon Press, United Kingdom, 1973).
- [31] Z. Wang, A. Marandi, K. Wen, R. L. Byer, and Y. Yamamoto, “Coherent Ising machine based on degenerate optical parametric oscillators,” *Phys. Rev. A* **88**, 063853 (2013).
- [32] A. Marandi, Z. Wang, K. Takata, R. L. Byer, and Y. Yamamoto, “Network of time-multiplexed optical parametric oscillators as a coherent Ising machine,” *Nat. Photonics* **8**, 937 (2014).
- [33] L. McMahon Peter, A. Marandi, Y. Haribara, R. Hamerly, C. Langrock, S. Tamate, T. Inagaki, H. Takesue, S. Utsunomiya, K. Aihara, L. Byer Robert, M. M. Fejer, H. Mabuchi, and Y. Yamamoto, “A fully programmable 100-spin coherent Ising machine with all-to-all connections,” *Science* **354**, 614 (2016).
- [34] T. Inagaki, Y. Haribara, K. Igarashi, T. Sonobe, S. Tamate, T. Honjo, A. Marandi, L. McMahon Peter, T. Umeki, K. Enbutsu, O. Tadanaga, H. Takenouchi, K. Aihara, K.-i. Kawarabayashi, K. Inoue, S. Utsunomiya, and H. Takesue, “A coherent Ising machine for 2000-node optimization problems,” *Science* **354**, 603 (2016).
- [35] A. Marandi, N. C. Leindecker, K. L. Vodopyanov, and R. L. Byer, “All-optical quantum random bit generation from intrinsically binary phase of parametric oscillators,” *Opt. Exp.* **20**, 19322 (2012).
- [36] M. A. Nielsen, and I. Chuang, *Quantum computation and quantum information* (Cambridge University Press, 2010)
- [37] P. L. Montgomery, “Modular multiplication without trial division,” *Math. Comput.* **44**, 519-521 (1985).
- [38] C. K. Koc, T. Acar, and B. S. Kaliski, “Analyzing and comparing Montgomery multiplication algorithms,” *IEEE Micro* **16**, 26-33 (1996).